



# *In situ* thermodiffraction to monitor synthesis and thermolysis of hydrazine borane-based materials



Romain Moury<sup>a,1</sup>, Koen Robeyns<sup>b</sup>, Yaroslav Filinchuk<sup>b</sup>, Philippe Miele<sup>a</sup>,  
Umit B. Demirci<sup>a,\*</sup>

<sup>a</sup> IEM (Institut Européen des Membranes), UMR 5635, Université de Montpellier, CNRS, ENSCM, Place Eugène Bataillon, CC047, F-34095, Montpellier, France

<sup>b</sup> Institute of Condensed Matter and Nanosciences, Université Catholique de Louvain, Place L. Pasteur 1, 1348 Louvain-la-Neuve, Belgium

## ARTICLE INFO

### Article history:

Received 3 September 2015

Received in revised form

13 October 2015

Accepted 7 November 2015

Available online 12 November 2015

### Keywords:

Hydrazine borane

Hydrogen storage materials

*In situ* X-ray diffraction

Lithium hydrazinidoborane

Sodium hydrazinidoborane

## ABSTRACT

Hydrazine borane  $N_2H_4BH_3$  (HB) and its alkali metal derivatives, *i.e.* sodium hydrazinidoborane  $NaN_2H_3BH_3$  (NaHB) and lithium hydrazinidoborane  $\beta$ - $LiN_2H_3BH_3$  ( $\beta$ -LiHB), are novel materials under investigation for solid-state chemical hydrogen storage. Herein, we report *in situ* thermodiffraction experiments developed to monitor synthesis of NaHB at low temperatures (from  $-173$  °C) and a thermolysis of each of the boranes, manifesting the following main observations. (i) Dehydrogenation of HB starts with the liquid phase and dehydrocoupling involves the formation of a crystalline intermediate (at  $90$ – $197$  °C). (ii) NaHB forms from  $-38$  °C, melts at *ca.*  $60$  °C, and decomposes upon melting at higher temperatures. (iii)  $\beta$ -LiHB dehydrogenates to a small extent starting from  $40$  °C, but mostly transforms to the high-temperature phase  $\alpha$ -LiHB at  $91$  °C; up to around  $150$  °C, the two crystalline phases dehydrogenate according to a complex stepwise mechanism. Our results help in gaining insight in synthesis and thermolysis of the aforementioned novel hydrazine borane-based materials.

© 2015 Elsevier B.V. All rights reserved.

## 1. Introduction

In the field of solid-state chemical hydrogen storage, boron- and nitrogen-containing materials are attractive hydrogen-dense compounds although the storage is irreversible in practical and acceptable conditions (in terms of temperature and pressure of hydrogen) [1]. The most typical example is ammonia borane  $NH_3BH_3$ , which carries 19.5 wt% of both protic and hydridic hydrogens ( $3 H^{\delta+}$  vs.  $3 H^{\delta-}$ ). Under heating, it melts at around  $100$  °C and then decomposes. The decomposition is stepwise over the range  $100$ – $200$  °C, with liberation of  $1 + 1$  equiv.  $H_2$  in two successive steps and of large amounts of undesired gaseous by-products such as ammonia, borazine and diborane especially during the second decomposition step [2]. To improve the dehydrogenation properties of ammonia borane, different destabilization strategies have been investigated so far: *i.e.* solvation in organic solvent/ionic liquid with and without the presence of homogeneous catalyst [3–5]; chemical doping with solid-state oxidant or

hydride [6,7]; confinement into the porosity of host material (scaffold) [8]; and chemical modification with synthesis of amido-borane derivatives [9].

Another example of boron- and nitrogen-containing materials is hydrazine borane  $N_2H_4BH_3$  (15.4 wt% H; with  $4 H^{\delta+}$  vs.  $3 H^{\delta-}$ ). It can be considered as a derivative of ammonia borane where the  $NH_3$  moiety is substituted by  $N_2H_4$ . Hydrazine borane (denoted HB) was discovered in the 1960s [10] but was thereafter little studied [11]. It gained new interest in the recent years [12]. In 2009, Hügler et al. [13] showed that an equimolar mixture of lithium hydride LiH and HB, with a balanced number of protic and hydridic hydrogen atoms ( $4 H^{\delta+}$  vs.  $4 H^{\delta-}$ ), is able to dehydrogenate in suitable conditions. In 2012, Moury et al. [14] confirmed the unsuitability of hydrazine borane in pristine state for solid-state chemical hydrogen storage whereas in 2011 Hannauer et al. [15] showed a real potential for liquid-state chemical hydrogen storage (*i.e.* catalytic dehydrogenation in hydrolysis conditions). However, HB has not been eliminated as a candidate solid-state chemical hydrogen storage material by the fact that like ammonia borane it can be chemically modified towards formation of derivatives [11].

By the reaction with an alkali metal hydride MH (with  $M = Li, Na$  and  $K$ ), HB can be transformed into an alkali metal hydrazinidoborane  $MN_2H_3BH_3$ . The first derivative,  $LiN_2H_3BH_3$  (11.6 wt% H;

\* Corresponding author.

E-mail address: [umit.demirci@umontpellier.fr](mailto:umit.demirci@umontpellier.fr) (U.B. Demirci).

<sup>1</sup> Present address: Max-Planck-Institut für Kohlenforschung, Kaiser-Wilhelm-Platz 1, 45470 Mülheim, Germany.

denoted  $\alpha$ -LiHB) was reported by Wu et al. [16]. Another polymorph,  $\beta$ -LiHB, was reported by Moury et al. [17]. The former is the high-temperature phase, while the latter is the low-temperature one, the transition taking place at about 90 °C. Both polymorphs can be synthesized by ball-milling but in different conditions [17]. An accurate determination of the phase transition temperature between these two phases is one of the objectives of the present work.

Sodium hydrazinidoborane  $\text{NaN}_2\text{H}_3\text{BH}_3$  (8.9 wt% H; denoted NaHB) [18] and potassium hydrazinidoborane  $\text{KN}_2\text{H}_3\text{BH}_3$  (7.2 wt% H; denoted KHB) were also reported [19] as derivatives of HB. Nevertheless, the reaction of NaH and KH with HB is exothermic, even highly exothermic with the latter hydride, taking an explosive nature. Synthesis of  $\text{KN}_2\text{H}_3\text{BH}_3$  can be conducted in safe conditions in an autoclave [19]. With respect to the synthesis of  $\text{NaN}_2\text{H}_3\text{BH}_3$ , it can be done in safe conditions by milling both reactants in a jar kept at low temperatures (e.g. by immersing the jar in liquid nitrogen) [18]. Determining a “safe” temperature of the reaction between NaH and HB towards the formation of NaHB and, for that, developing a novel *in situ* method are the objectives of the present work.

The aforementioned hydrazinidoborane derivatives possess an equal number of protic and hydridic hydrogen atoms ( $3\text{H}^{\delta+}$  vs.  $3\text{H}^{\delta-}$ ). Thus, the dehydrogenation could theoretically reach high yield, probably quantitative, likely at moderate temperatures. Indeed, the hydrazinidoboranes have shown much better dehydrogenation kinetics than pristine HB [16–19]. For example, LiHB is able to release 9.3 wt% H (out of a maximum of 11.6 wt% H) under heating at 130 °C for 1 h [16] and NaHB liberates 8.8 wt% H (out of a maximum of 8.9 wt%) at 100 °C in less than 10 min [18]. Accordingly, alkali metal hydrazinidoboranes are positioned as potential candidates for solid-state chemical hydrogen storage. Nonetheless, technological application and viability of these compounds is strongly dependent on recyclability of the solid residues to regenerate the starting materials or at least a compound like sodium/lithium borohydride, ammonia borane or HB. A promising way is reduction by using hydrazine in ammonia medium, which has already shown to be efficient for hydrogenating polyborazylene into ammonia borane [20,21]. Recyclability is certainly the most challenging issue in the field.

The present work is dedicated to *in situ* thermodiffraction of HB,  $\beta$ -LiHB and NaHB. Specifically, we aim at gaining more insight, from a crystallographic point of view, into (i) the synthesis of NaHB from  $-173$  °C to ambient conditions followed by a novel *in situ* method, (ii) the thermal decomposition of HB from 20 °C to 220 °C, paying attention to possible formation of an intermediate, (iii) the phase transition  $\beta$ -LiHB  $\rightarrow$   $\alpha$ -LiHB over the range 90–155 °C as well as the thermal decomposition of these phases from 20 °C to 200 °C, and (iv) the thermal decomposition of NaHB from 20 °C to 200 °C.

## 2. Experimental

Sodium borohydride  $\text{NaBH}_4$  (Acros, 99%), hydrazine hemisulfate  $\text{N}_2\text{H}_4 \cdot 1/2(\text{SO}_4)$  (Sigma–Aldrich, >99%), anhydrous 1,4-dioxane  $\text{C}_4\text{H}_8\text{O}_2$  (Sigma–Aldrich, >99%), lithium hydride LiH (Sigma–Aldrich, 95%) and sodium hydride NaH (Sigma–Aldrich, 95%) were used as-received, stored and handled in an argon-filled glove box (MBraun M200B,  $\text{H}_2\text{O} \leq 0.1$  ppm,  $\text{O}_2 \leq 0.1$  ppm).

Hydrazine borane  $\text{N}_2\text{H}_4\text{BH}_3$  (purity  $\geq 99\%$ ) was synthesized from  $\text{NaBH}_4$  and  $\text{N}_2\text{H}_4 \cdot 1/2(\text{SO}_4)$  in 1,4-dioxane following an optimized procedure described in details elsewhere [14]. The synthesis of sodium hydrazinidoborane ( $\text{NaN}_2\text{H}_3\text{BH}_3$ ) is described in details elsewhere [18]. In the present study, the procedure was adapted to *in situ* XRD. In the argon-filled glove box, equimolar amounts of NaH and  $\text{N}_2\text{H}_4\text{BH}_3$  were introduced in a stainless steel milling jar while taking care not to put the reactants into contact; they were

separated by 5 stainless steel balls ( $\varnothing$  70 mm). The jar was carefully taken out the glove box and put in a Dewar container filled with liquid nitrogen ( $-196$  °C) for 1 h. Then, the cold jar was placed in the ball mill (FRITSH Pulverisette 7 Premium Line) and the mixture was milled for 5 min at 250 rpm. The jar was placed in liquid nitrogen once again and then placed in a nitrogen glove box. Several glass capillaries ( $\varnothing$  0.7 mm) were filled with the mixture while keeping the temperature close to  $-196$  °C. The samples in capillaries were finally analyzed by XRD.

Lithium hydrazinidoborane has two known polymorphs: the low-temperature phase  $\beta$ -LiHB [17] and the high-temperature  $\alpha$ -LiHB [16]. In the present work,  $\beta$ -LiHB was prepared from equimolar amounts of LiH and  $\text{N}_2\text{H}_4\text{BH}_3$  by ball-milling in the following conditions: ambient temperature; PM100 ball mill from RETSCH; balls-to-reactants weight ratio of  $\sim 100$ ; 180 min by alternating 10 min milling at 200 rpm with 20 min break. With respect to  $\alpha$ -LiHB, it was prepared with another ball mill (FRITSH Pulverisette 7 Premium Line) and by applying 3 different cycles at ambient temperature: 180 min of milling at 200 rpm for 10 min alternated with 20 min break; 160 min of milling at 250 rpm for 10 min with 10 min break; and, 360 min of milling at 300 rpm for 10 min with 20 min break.

The synthesis of NaHB from NaH and  $\text{N}_2\text{H}_4\text{BH}_3$  has to be done at low temperatures [18]. To precisely define the reaction temperature, the pressure in the milling jar was monitored from  $-100$  °C to 20 °C and the gas composition was analyzed at the end of the experiment. Typically, a jar equipped with a quick connect gas outlet was used in milling under the conditions reported above. The variations in pressure and temperature were recorded. The jar was connected to a gas chromatograph (GC; Shimadzu, GC-14B; Column Chromosorb 103; 40 °C; detector TCD; 2250 points recorded every 0.4 s for 15 min) and upon the completion of the reaction, the jar atmosphere was analyzed. The GC results showed the presence of  $\text{H}_2$  (retention time of 1.57 min) only. No other by-product was found.

The synthesis of NaHB was also followed by *in situ* XRD. An X-ray diffractometer, with an image plate detector MAR345 positioned at 250 mm, a Rigaku rotated anode generator and a molybdenum radiation ( $\lambda_{\text{K}\alpha} = 0.71069$  Å), was used. The detector geometry was calibrated with the  $\text{LaB}_6$  standard. The temperature was controlled using a programmable gas blower Oxford Cryostream 700. The temperature was first set at  $-173$  °C and then increased at  $0.5$  °C  $\text{min}^{-1}$ . The same diffractometer was used to verify the successful synthesis of  $\alpha$ -LiHB.

The thermal behavior of HB, NaHB and  $\beta$ -LiHB was studied using synchrotron radiation at the BM01-A beamline (ESRF). The wavelength was  $\lambda = 0.69405$  Å. A 2D Pilatus detector positioned at 411 mm from the sample was used. The detector geometry was calibrated with the  $\text{LaB}_6$  standard. The temperature was controlled using a Cyberstar hot blower. The analysis was performed from room temperature to 250 °C with a heating rate of  $5$  °C  $\text{min}^{-1}$ . The thermal behavior of HB was also studied by thermogravimetric analysis (TGA) coupled to mass spectrometry (MS). The measurements were performed in an argon-filled glove box using a Rigaku TG8120 TGA (3 mg of product in a platinum crucible;  $2$  °C  $\text{min}^{-1}$ ) and an M-QA200TS MS under helium flux respectively. The thermal behavior of NaHB and  $\beta$ -LiHB are reported elsewhere [17,18].

## 3. Results and discussion

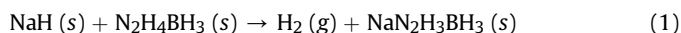
### 3.1. *In situ* monitoring of NaHB synthesis

At ambient temperature and under argon atmosphere, NaH and HB spontaneously react [18]. The reaction can be controlled by gradually increasing the temperature. This interesting feature was used to successfully develop an *in situ* approach to monitor the low-

temperature reaction between both reactants. Fig. 1 shows the *in situ* XRD patterns collected from  $-173\text{ }^{\circ}\text{C}$ . Up to  $-38\text{ }^{\circ}\text{C}$ , there is no apparent change in the diffraction peaks of NaH and HB, suggesting no reaction. Additional diffraction peaks can be observed from  $-88\text{ }^{\circ}\text{C}$  to  $-38\text{ }^{\circ}\text{C}$ ; they are due to ice  $I_h$  ( $P6_3/mmc$ ). Above  $-38\text{ }^{\circ}\text{C}$ , the intensity of the peaks of NaH and HB decays and additional peaks ascribed to NaHB appear. The latter one increases in intensity with temperature. At  $11\text{ }^{\circ}\text{C}$ , there are no more crystalline reactants left. All of the diffraction peaks belong to NaHB and their intensity rises with the increase of the temperature up to  $25\text{ }^{\circ}\text{C}$ .

Pressure measurement was performed during the synthesis of NaHB. The gas composition was analyzed by GC afterwards:  $\text{H}_2$  was detected; no trace of by-product was observed. By using the ideal gas law, the final pressure was recalculated to the number of moles of the generated  $\text{H}_2$ , yielding 1 mol  $\text{H}_2$  per mol  $\text{N}_2\text{H}_4\text{BH}_3$ . The pressure variation was then qualitatively correlated with the XRD observations. Because of temperature gradients in the jar, it is not relevant to calculate a number of moles from the pressure data [22]. Fig. 2 shows the pressure variation as a function of the temperature; the intensity variation of the peak at  $2\theta = 9.0^{\circ}$  from NaHB is also shown as a function of the temperature. From  $-100$  and  $-85\text{ }^{\circ}\text{C}$ , there is apparently no reaction between the reactants. Between  $-85\text{ }^{\circ}\text{C}$  and  $-81\text{ }^{\circ}\text{C}$ , there is a pressure step, suggesting some interaction/reaction between NaH and HB. Then, up to  $-38\text{ }^{\circ}\text{C}$ , there is almost no reaction. Above  $-38\text{ }^{\circ}\text{C}$ , NaHB forms. The amount of NaHB then increases along with the  $\text{H}_2$  pressure. From  $-20\text{ }^{\circ}\text{C}$  to  $0\text{ }^{\circ}\text{C}$ , the rate of formation of NaHB and  $\text{H}_2$  would be slow. Above  $0\text{ }^{\circ}\text{C}$ , the pressure increase is faster and may be attributed to the increase in the effective gas temperature inside the milling jar. Note that from  $-38\text{ }^{\circ}\text{C}$  the variation of the pressure (i.e. the  $\text{H}_2$  evolution) is parallel to that of the intensity of the diffraction peak of NaHB, suggesting that no intermediate complex (even liquid or amorphous) forms.

To be in safe conditions, the synthesis of NaHB must be done by milling at temperatures lower than  $-38\text{ }^{\circ}\text{C}$ . The reaction between NaH and HB is direct and leads to the formation of pure NaHB and 1 equiv.  $\text{H}_2$  according to the following reaction:



### 3.2. *In situ* monitoring of thermolysis

#### 3.2.1. Hydrazine borane

The thermal decomposition of HB was followed by *in situ* XRD over the range  $20\text{--}220\text{ }^{\circ}\text{C}$ . It was compared to the TGA-MS results.

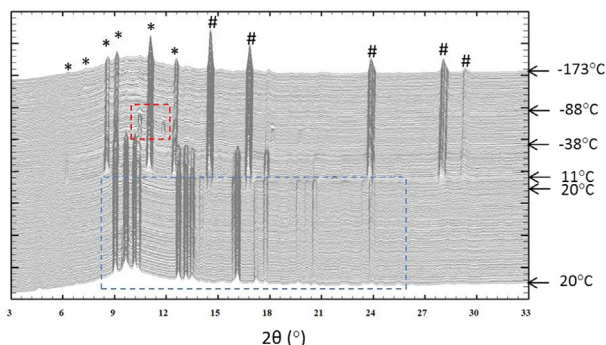


Fig. 1. Reaction between NaH (#) and  $\text{N}_2\text{H}_4\text{BH}_3$  (\*) followed by *in situ* XRD ( $\lambda = 0.71069\text{ \AA}$ ). The red square indicates the appearance of ice  $I_h$  ( $P6_3/mmc$ ). The blue square shows the NaHB crystalline phase. (For interpretation of the references to colour in this figure legend, the reader is referred to the web version of this article.)

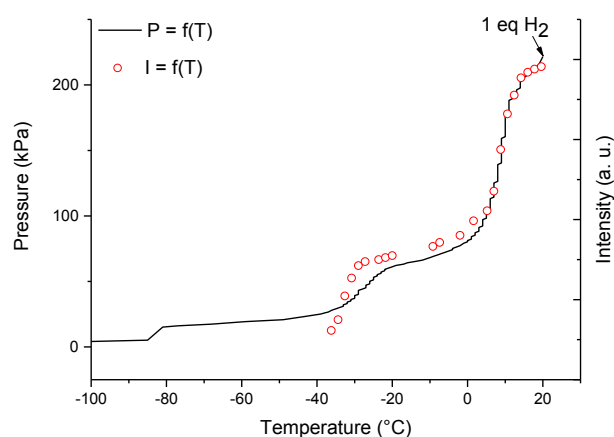


Fig. 2. Comparison between the pressure (due to  $\text{H}_2$ ) measured during the synthesis of NaHB (black solid line) and, evolution of the integrated intensity of the diffraction peak  $2\theta = 9.0^{\circ}$  for NaHB (red circles). (For interpretation of the references to colour in this figure legend, the reader is referred to the web version of this article.)

The results are presented in Figs. 3 and 4 respectively. The crystal phase of HB disappears slowly up to  $37\text{ }^{\circ}\text{C}$  and then more quickly over the range of  $37\text{--}44\text{ }^{\circ}\text{C}$ . Within this range, the lattice parameters vary linearly with temperature increase (Fig. 5a); they all follow the same trends but the thermal expansion coefficients are different (Table 1).

At  $44\text{ }^{\circ}\text{C}$ , the diffraction peaks of HB vanish completely, which corresponds to melting, but HB dehydrogenates at higher temperature ( $65\text{ }^{\circ}\text{C}$ ) [14]. This suggests that dehydrogenation starts with the liquid phase of the HB.

The baseline of the XRD patterns deviates towards higher intensity from  $65\text{ }^{\circ}\text{C}$ , then reaches maximum at  $71\text{ }^{\circ}\text{C}$  and finally deviates to lower intensity to become constant at  $174\text{ }^{\circ}\text{C}$ . This is consistent with the formation of polymeric species upon melting and subsequent dehydrocoupling of the HB molecules [10].

At  $90\text{ }^{\circ}\text{C}$ , a diffraction peak at  $2\theta = 7.4^{\circ}$  appears. It disappears at  $197\text{ }^{\circ}\text{C}$ . This is indicative of a certain degree of order in the decomposition intermediate. As decomposition of HB leads to solid residue with boron in  $\text{sp}^2$  hybridization [14], the formation of flat aromatic-like molecules under heating may be suggested. Parallels

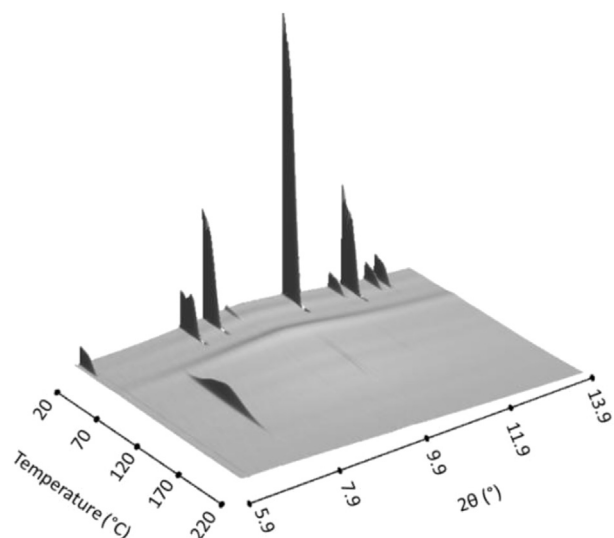
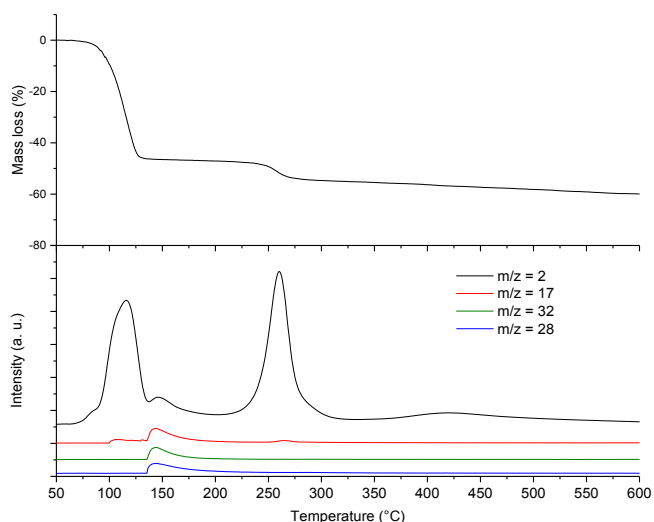


Fig. 3. Thermal decomposition of HB followed by *in situ* XRD ( $\lambda = 0.69405\text{ \AA}$ ).



**Fig. 4.** TGA (up) and MS results (down) of HB, with  $m/z = 2$  ( $H_2$ ), 17 ( $NH_3$ ), 28 ( $N_2$ ) and 32 ( $N_2H_4$ ).

with the thermolytic decomposition of ammonia borane can be drawn. Indeed, ammonia borane decomposes under heating with formation of borazine that is able to polycondensate to form polyborazylene [23–25]. A mesophase may be also obtained with special treatment of liquid borazine [26]. Henceforth, one may tentatively propose that thermolytic decomposition of HB would take place as follows: (i) formation of aromatic-like molecules in the liquid phase and subsequent polymerization into oligomeric structures at 44–90 °C; (ii) alignment of the oligomer chains in one direction due to stacking interactions, thus formation of a mesophase (this is especially supported by the degree of order observed in the XRD patterns from 90 to 197 °C); (iii) breaking of the mesophase to form solid polymers (mixture of linear polyborazylene-like polymers [14]) over the range 197–220 °C.

### 3.2.2. Lithium hydrazinidoborane

As earlier reported [17],  $\beta$ -LiHB dehydrogenates starting from ca. 40 °C. It is a three-step process up to 144 °C, with successive mass losses of 1.2 wt% at 40–104 °C due to  $H_2$  and  $N_2$ , 2.2 wt% at 104–127 °C due to  $H_2$ , and 4.4 wt% at 127–144 °C due to  $H_2$ .

The thermal decomposition of  $\beta$ -LiHB was thus followed by *in situ* XRD over the range 20–155 °C. The results are presented in Fig. 6. The phase transition from the low-temperature phase  $\beta$ -LiHB

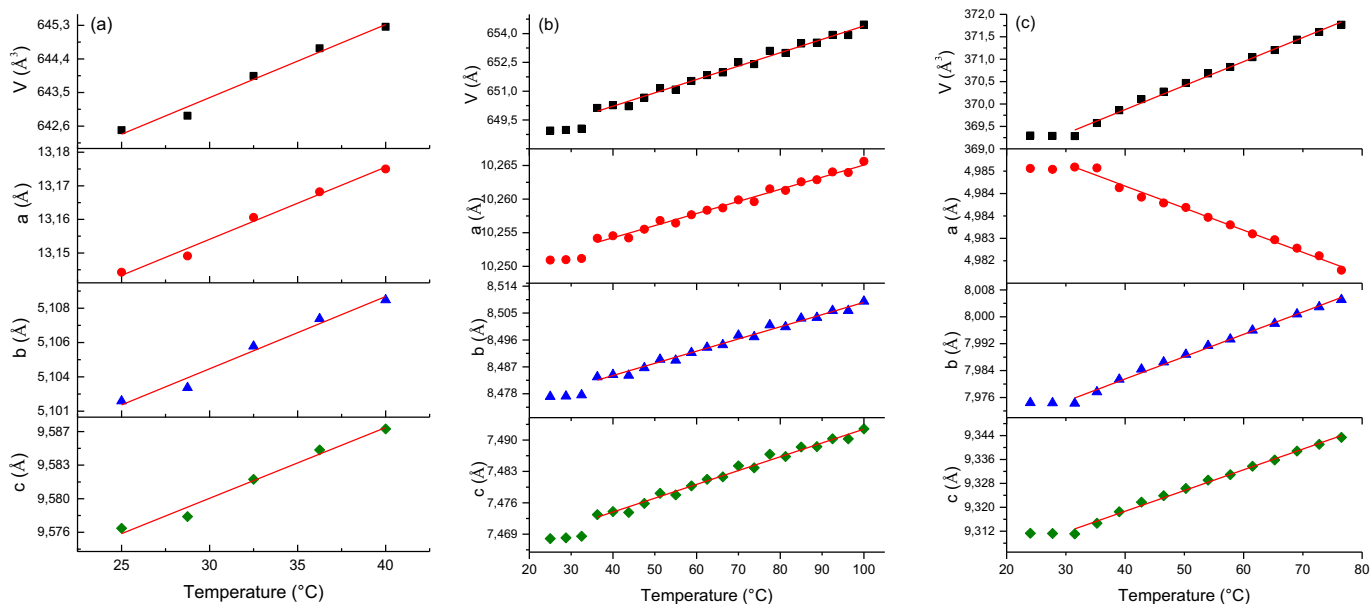


**Fig. 5.** Evolution of the cell parameters of (a) HB, (b)  $\beta$ -LiHB and (c) NaHB as a function of the temperature. The patterns were refined from the thermal *in situ* XRD experiments. The solid red straight lines represent the linear fits (cf. text and Table 1). (For interpretation of the references to colour in this figure legend, the reader is referred to the web version of this article.)

**Table 1**

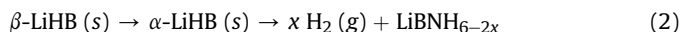
Equations of the evolution of the cell parameters as a function of the temperature for HB, NaHB and  $\beta$ -LiHB. For each equation, the standard error slope and the standard error intercept are given in brackets in the cell below the equation.

Cell parameters	HB	NaHB	$\beta$ -LiHB
$V$ ( $\text{\AA}^3$ )	$1.96 \cdot 10^{-3} \times T + 637.489$ ( $1.10 \cdot 10^{-4}$ ) ( $5.10 \cdot 10^{-1}$ )	$5.36 \cdot 10^{-2} \times T + 367.733$ ( $1.10 \cdot 10^{-3}$ ) ( $7.10 \cdot 10^{-2}$ )	$6.96 \cdot 10^{-2} \times T + 647.436$ ( $2.10 \cdot 10^{-3}$ ) ( $1.3 \cdot 10^{-1}$ )
$a$ ( $\text{\AA}$ )	$1.74 \cdot 10^{-3} \times T + 13.106$ ( $1.1 \cdot 10^{-4}$ ) ( $3.7 \cdot 10^{-3}$ )	$-4.93 \cdot 10^{-4} \times T + 4.986$ ( $1.3 \cdot 10^{-6}$ ) ( $7.9 \cdot 10^{-5}$ )	$1.80 \cdot 10^{-4} \times T + 10.247$ ( $5.5 \cdot 10^{-6}$ ) ( $3.9 \cdot 10^{-4}$ )
$b$ ( $\text{\AA}$ )	$4.84 \cdot 10^{-4} \times T + 5.090$ ( $4.2 \cdot 10^{-5}$ ) ( $1.4 \cdot 10^{-3}$ )	$6.64 \cdot 10^{-4} \times T + 7.955$ ( $1.5 \cdot 10^{-5}$ ) ( $8.3 \cdot 10^{-4}$ )	$4.08 \cdot 10^{-5} \times T + 8.468$ ( $1.1 \cdot 10^{-6}$ ) ( $7.8 \cdot 10^{-4}$ )
$c$ ( $\text{\AA}$ )	$7.37 \cdot 10^{-4} \times T + 9.557$ ( $6.10 \cdot 10^{-5}$ ) ( $2.10 \cdot 10^{-3}$ )	$6.94 \cdot 10^{-4} \times T + 9.291$ ( $1.5 \cdot 10^{-5}$ ) ( $8.6 \cdot 10^{-4}$ )	$3.08 \cdot 10^{-4} \times T + 7.462$ ( $8.7 \cdot 10^{-6}$ ) ( $6.2 \cdot 10^{-4}$ )
$\beta$ (°)		$2.57 \cdot 10^{-3} \times T + 93.74$ ( $6.5 \cdot 10^{-5}$ ) ( $3.10 \cdot 10^{-2}$ )	

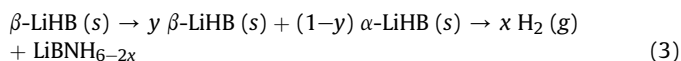
*Pbca* (No. 61) to the high-temperature phase  $\alpha$ -LiHB *P2<sub>1</sub>/c* [14] starts at 91 °C. Both phases coexist over the range of 91–137 °C, suggesting a first-order phase transition associated with a nucleation process where a temperature hysteresis is expected. The cell parameters of  $\beta$ -LiHB vary linearly but anisotropically with temperature (Fig. 5b, Table 1). The diffraction peaks of  $\beta$ -LiHB and  $\alpha$ -LiHB vanish at 147 and 151 °C respectively. No crystalline product of the decomposition was detected over the studied temperature range.

The high-temperature phase  $\alpha$ -LiHB can be obtained at ambient conditions [16]. In the present work, we obtained  $\alpha$ -LiHB by heating the low-temperature phase  $\beta$ -LiHB at 95 °C for 2 h under inert atmosphere, followed by slow cooling. Only  $\alpha$ -LiHB diffracted (the pattern is not shown), evidencing an irreversible phase transition with a high-temperature hysteresis. The phase  $\alpha$ -LiHB is thus metastable [27]. The metastability of this borane may be explained by the small size of the lithium cation (as with the lithium amidoborane phases, *i.e.*  $\alpha$ -LiNH<sub>2</sub>BH<sub>3</sub> and  $\beta$ -LiNH<sub>2</sub>BH<sub>3</sub>) [28], and/or crystal size effect (as with tetragonal zirconia ZrO<sub>2</sub>) [29,30]. The crystallite sizes of both phases were determined by Rietveld and micro-structure refinements of the XRD patterns (Fig. 7). Mean crystallite sizes of 53.3 and 23.9 nm were found for  $\beta$ -LiHB and  $\alpha$ -LiHB respectively.

Accordingly, the results reported above lead to four concluding remarks. (1) The phase  $\beta$ -LiHB transforms into  $\alpha$ -LiHB from 91 °C. (2) Both phases may contribute to the stepwise dehydrogenation of the solid over the range 91–155 °C. (3) It is inadequate to state the following sequence:



As most likely both phases concomitantly dehydrogenate, the phase  $\beta$ -LiHB is able to lose some H<sub>2</sub> below 91 °C, bringing us the following scheme:



(4) Importantly, and unlike for HB and NaHB, the dehydrogenation of LiHB mainly occurs from the crystalline phase. This could be attributed to stronger intermolecular forces within the structure [19].

### 3.2.3. Sodium hydrazinidoborane

Under heating at 2 °C min<sup>-1</sup>, NaHB starts to dehydrogenate from *ca.* 60 °C, releasing 7.6 wt% H<sub>2</sub> (with traces of N<sub>2</sub>, NH<sub>3</sub> and N<sub>2</sub>H<sub>4</sub>) up to 150 °C [18]. The thermal dehydrogenation of NaHB was followed by *in situ* XRD over the range of 20–200 °C. The results are presented in Fig. 8. The disappearance of the diffraction peaks may be

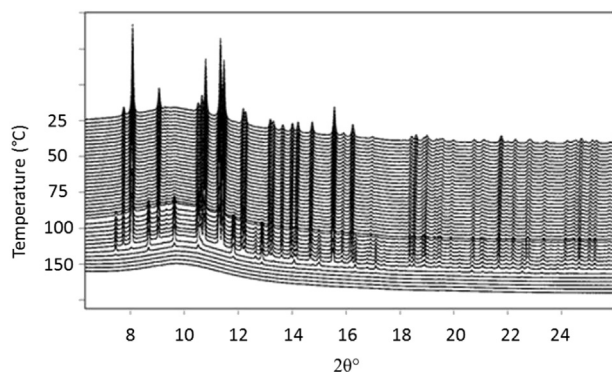


Fig. 6. Thermal decomposition of  $\beta$ -LiHB followed by *in situ* XRD ( $\lambda = 0.69405$  Å).

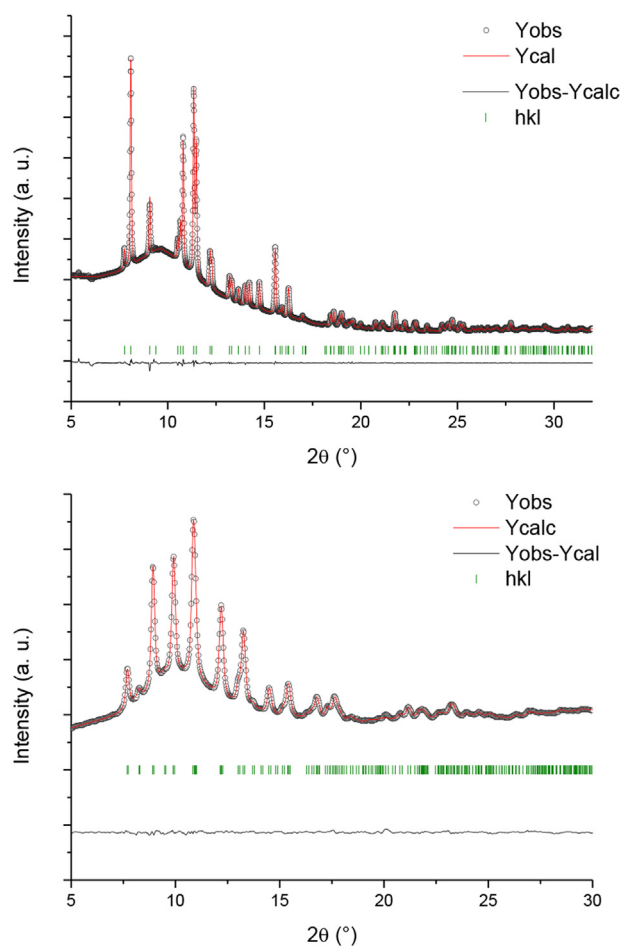


Fig. 7. Microstructure refinements of (top)  $\beta$ -LiHB and (bottom)  $\alpha$ -LiHB, in ambient conditions ( $\lambda = 0.69405$  Å for  $\beta$ -LiHB and  $\lambda = 0.71069$  Å  $\alpha$ -LiHB).

seen as three-step process with different kinetics: fast from 30 to 41 °C, slower at 41–61 °C and very fast above and up to 76 °C. The parameters and unit cell volume of NaHB varies linearly with temperature over 30–78 °C (Fig. 5c). The thermal expansion is anisotropic. The parameters *b* and *c* expand with approximately the same thermal expansion coefficient whereas the parameter *a* decreases (Table 1).

At 76 °C, no more crystal phase is observed, which is consistent with melting of NaHB, earlier reported to occur at 75 °C [19]. Dehydrogenation of NaHB takes place mainly above 76 °C, namely from the amorphous phase. The examination of the baseline of the XRD patterns shows that the amount of the amorphous phase increases in terms of intensity while that of the crystalline phase decreases. The fraction of the amorphous phase reaches its maximum at 94 °C. Then, it decreases until it becomes constant at 100 °C. Unlike HB, no formation of intermediate crystalline phase is observed during the dehydrogenation of NaHB.

### 3.3. Summary

Hydrazine borane is the precursor in synthesis of  $\beta$ -LiHB and  $\alpha$ -LiHB. Both phases are obtained by ball-milling in different conditions [16,17] and the successful syntheses can be verified post-reaction by *ex situ* XRD and solid-state NMR. Hydrazine borane is also the precursor to NaHB; it is highly reactive with respect to NaH, a simple contact leading to an exothermic reaction. The synthesis

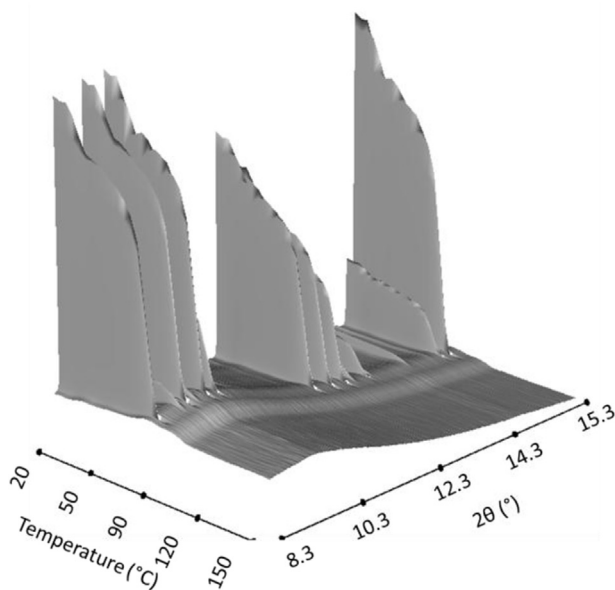
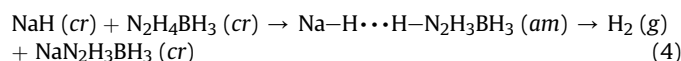


Fig. 8. Thermal decomposition of NaHB followed by *in situ* XRD ( $\lambda = 0.69405 \text{ \AA}$ ).

can be done successfully at low temperatures and the formation of NaHB can be monitored by temperature-variable *in situ* XRD and concomitantly the evolution of  $\text{H}_2$  followed from the pressure variation. In this way, it has been demonstrated that HB and NaH react starting from  $-38 \text{ }^\circ\text{C}$ . The reaction is direct with evolution of 1 equiv.  $\text{H}_2$  (Eq. (1)) and with a formation of crystalline NaHB. At subzero temperatures, the rate of formation is rather low, the heat of the reaction being efficiently taken away, but above  $>0 \text{ }^\circ\text{C}$ – $60\%$  of  $\text{H}_2$  is liberated with much faster kinetics because of the thermal activation (auto-catalysis). From the temperature-dependent XRD patterns, it can be assumed that synthesis of NaHB comprises a step of amorphization of both reactants prior to the reaction (Fig. 9):



Under the constant heating rate, the aforementioned hydrazine borane-based materials decompose well below  $100 \text{ }^\circ\text{C}$ . The decomposition mechanisms seem to be quite different. HB melts at

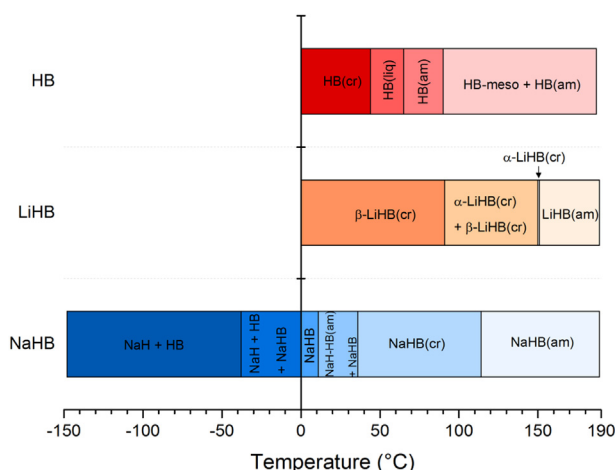
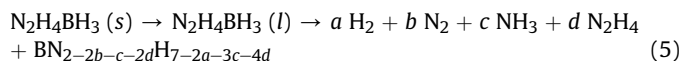
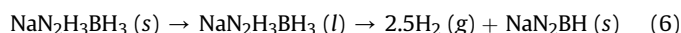


Fig. 9. Evolution of HB, LiHB and NaHB over the temperature range of  $[-150]$ – $[190]^\circ\text{C}$ .

$44 \text{ }^\circ\text{C}$  and it is the liquid phase of HB that dehydrogenates from  $65 \text{ }^\circ\text{C}$ . Dehydrocoupling of HB leads to polymeric solids, but one of them shows a certain degree of order at  $90$ – $197 \text{ }^\circ\text{C}$  with appearance of diffraction peaks (Fig. 9):



The dehydrogenation of  $\beta$ -LiHB is complex. Small part of crystalline  $\beta$ -LiHB dehydrogenates over the range  $40$ – $91 \text{ }^\circ\text{C}$ . At  $91 \text{ }^\circ\text{C}$ ,  $\beta$ -LiHB transforms to  $\alpha$ -LiHB and both phases coexist up to *ca.*  $150 \text{ }^\circ\text{C}$ . Dehydrogenation at  $91$ – $150 \text{ }^\circ\text{C}$  may thus be explained according to either the sequence shown by Eq. (2) or that displayed by Eq. (3), namely by the dehydrogenation of  $\alpha$ -LiHB only or of both phases simultaneously. Whatever the path, dehydrogenation takes place from the crystalline phases (Fig. 9). With respect to dehydrogenation of NaHB, it is comparable to that of HB, with melting at  $75 \text{ }^\circ\text{C}$ , subsequent dehydrogenation and formation of an amorphous solid (Fig. 9):



#### 4. Conclusion

*In situ* XRD was shown to be an efficient tool to monitor synthesis of NaHB and thermal decomposition/dehydrogenation of HB,  $\beta$ -LiHB and NaHB, gaining insight about these processes. For example, synthesis of NaHB in safe conditions from HB and NaH can be achieved at low temperatures, ideally at  $-38 \text{ }^\circ\text{C}$ . The reaction between HB and NaH leads to the formation of crystalline NaHB and 1 mol  $\text{H}_2$  per mole of reactant ( $\text{H}_2$  evolution was followed by the pressure in the jar). Temperatures higher than  $0 \text{ }^\circ\text{C}$  have to be strictly avoided because of the exothermicity of the reaction, thus auto-catalyzed reaction and very fast hydrogen release.

*In situ* XRD has shown that the decompositions/dehydrogenations of the aforementioned hydrazine borane-based materials are different and complex. With HB, this is the liquid phase (melting at  $44 \text{ }^\circ\text{C}$ ) that decomposes from  $65 \text{ }^\circ\text{C}$ . A polymeric residue, with a certain degree of order, forms. The derivative LiHB has two crystalline phases. The low-temperature one  $\beta$ -LiHB dehydrogenates to a small extent starting from  $40 \text{ }^\circ\text{C}$  and transforms to the high-temperature phase  $\alpha$ -LiHB at  $91 \text{ }^\circ\text{C}$ . Then, both phases coexist up to *ca.*  $150 \text{ }^\circ\text{C}$ , and dehydrogenation occurs likely both from  $\beta$ -LiHB and  $\alpha$ -LiHB. Further works (e.g. isotopic labeling) are required to gain more insight. With respect to NaHB, dehydrogenation of about 2.5 equiv.  $\text{H}_2$  takes place after melting ( $75 \text{ }^\circ\text{C}$ ) leading to an amorphous residue of the empirical formulas  $\text{NaN}_2\text{BH}$ .

*In situ* XRD has been the first step to gain insight about the decomposition/dehydrogenation mechanisms of the hydrazine borane-based materials. Further works focusing on e.g. *in situ* NMR (despite the complexity of identification of the thermolytic residues [13]) and isotopic labeling for LiHB are planned.

#### Acknowledgments

The authors acknowledge the support of the Direction Générale des Armées (DGA), the Centre National de la Recherche Scientifique (CNRS) and the Fonds de la Recherche Scientifique (FNRS). UBD and YF acknowledge the support of the COST Action MP1103 “nanostructured materials for solid-state hydrogen storage” for the short-term scientific mission given to RM. For the beam time allocation, the authors acknowledge SNBL, at the ESRF.

## References

- [1] L.H. Jepsen, M.B. Ley, Y.Su Lee, Y.W. Cho, M. Dornheim, J.O. Jensen, Y. Filinchuk, J.E. Jørgensen, F. Besenbacher, T.R. Jensen, Boron–nitrogen based hydrides and reactive composites for hydrogen storage, *Mater. Today* 17 (2014) 129–135.
- [2] V. Sit, R.A. Geanangel, W.W. Wendlandt, The thermal dissociation of ammonia borane, *Thermochim. Acta* 113 (1987) 379–382.
- [3] M.E. Bluhm, M.G. Bradley, R. Butterick III, U. Kusari, L.G. Sneddon, Amine-borane-based chemical hydrogen storage: enhanced ammonia borane dehydrogenation in ionic liquids, *J. Am. Chem. Soc.* 128 (2006) 7748–7749.
- [4] M.C. Denney, V. Pons, T.J. Hebden, D.M. Heinekey, K.I. Goldberg, Efficient catalysis of ammonia borane dehydrogenation, *J. Am. Chem. Soc.* 128 (2006) 12048–12049.
- [5] J.F. Kostka, R. Schellenberg, F. Baitalow, T. Smolinka, F. Mertens, Concentration-dependent dehydrogenation of ammonia-borane/triglyme mixtures, *Eur. J. Inorg. Chem.* 1 (2012) 49–54.
- [6] R. Benzoua, U.B. Demirci, R. Chiriac, F. Toche, P. Miele, Metal chloride-doped ammonia borane thermolysis: positive effect on induction period as well as hydrogen and borazine release, *Thermochim. Acta* 509 (2010) 81–86.
- [7] N. Nakagawa, S. Isobe, Y. Ikarashi, S. Ohnuki, AB–MH (Ammonia Borane–Metal Hydride) composites: systematic understanding of dehydrogenation properties, *J. Mater. Chem. A* 2 (2014) 3926–3931.
- [8] A. Gutowska, L. Li, Y. Shin, C.M. Wang, X.S. Li, J.C. Linehan, R.S. Scott, B.D. Kay, B. Schmid, W. Shaw, M. Gutowski, T. Autrey, Nanoscaffold mediates hydrogen release and the reactivity of ammonia borane, *Angew. Chem.* 117 (2005) 3644–3648.
- [9] H. Wu, W. Zhou, T. Yildirim, Alkali and alkaline-earth metal amidoboranes: structure, crystal chemistry, and hydrogen storage properties, *J. Am. Chem. Soc.* 130 (2008) 14834–14839.
- [10] V.J. Goubeau, E. Ricker, Borinhydrizin und seine pyrolyseprodukte, *Z. Anorg. Allg. Chem.* 310 (1961) 123–142.
- [11] R. Moury, U.B. Demirci, Hydrazine borane and hydrazinidoboranes as chemical hydrogen storage materials, *Energies* 8 (2015) 3118–3141.
- [12] N. Vinh-Son, S. Swinnen, M.H. Matus, M.T. Nguyen, D.A. Dixon, The effect of the NH<sub>2</sub> substituent on NH<sub>3</sub>: hydrazine as an alternative for ammonia in hydrogen release in the presence of boranes and alanes, *Phys. Chem. Chem. Phys.* 11 (2009) 6339–6344.
- [13] T. Hügler, M.F. Kühnel, D. Lentz, Hydrazine borane: a promising hydrogen storage material, *J. Am. Chem. Soc.* 131 (2009) 7444–7446.
- [14] R. Moury, G. Moussa, U.B. Demirci, J. Hannauer, S. Bernard, E. Petit, A. van der Lee, P. Miele, Hydrazine borane: synthesis, characterization, and application prospects in chemical hydrogen storage, *Phys. Chem. Chem. Phys.* 14 (2012) 1768–1777.
- [15] J. Hannauer, O. Akdim, U.B. Demirci, C. Geantet, J.M. Herrmann, P. Miele, Q. Xu, High-extent dehydrogenation of hydrazine borane N<sub>2</sub>H<sub>4</sub>BH<sub>3</sub> by hydrolysis of BH<sub>3</sub> and decomposition of N<sub>2</sub>H<sub>4</sub>, *Energy Environ. Sci.* 4 (2011) 3355–3358.
- [16] H. Wu, W. Zhou, F.E. Pinkerton, T.J. Udovic, T. Yildirim, J.J. Rush, Metal hydrazinoborane LiN<sub>2</sub>H<sub>3</sub>BH<sub>3</sub> and LiN<sub>2</sub>H<sub>3</sub>BH<sub>3</sub>-2N<sub>2</sub>H<sub>4</sub>BH<sub>3</sub>: crystal structures and high-extent dehydrogenation, *Energy Environ. Sci.* 5 (2012) 7531–7535.
- [17] R. Moury, U.B. Demirci, V. Ban, Y. Filinchuk, T. Ichikawa, L. Zeng, K. Goshome, P. Miele, Lithium hydrazinidoborane, a polymorphic material with potential for chemical hydrogen storage, *Chem. Mater.* 26 (2014) 3249–3255.
- [18] R. Moury, U.B. Demirci, T. Ichikawa, Y. Filinchuk, R. Chiriac, A. van der Lee, P. Miele, Sodium hydrazinidoborane, a chemical hydrogen storage material, *Chem. Sus. Chem.* 6 (2013) 667–673.
- [19] Y.S. Chua, Q. Pei, X. Ju, W. Zhou, T.J. Udovic, G. Wu, Z. Xiong, P. Chen, H. Wu, Alkali metal hydride modification on hydrazine borane for improved dehydrogenation, *J. Phys. Chem. C* 118 (2014) 11244–11251.
- [20] A.D. Sutton, A.K. Burrell, D.A. Dixon, E.B. Garner III, J.C. Gordon, T. Nakagawa, K.C. Ott, J.P. Robinson, M. Vasiliu, Regeneration of ammonia borane spent fuel by direct reaction with hydrazine and liquid ammonia, *Science* 331 (2011) 1426–1429.
- [21] O.T. Summerscales, J.C. Gordon, Regeneration of ammonia borane from spent fuel, *Dalton Trans.* 42 (2013) 10075–11084.
- [22] J. Zhang, F. Cuevas, W. Zaidi, J.P. Bonnet, L. Aymard, J.L. Bobet, M. Latroche, Highlighting of a single reaction path during reactive ball milling of Mg and TM by quantitative H<sub>2</sub> gas sorption analysis to form ternary complex hydrides (TM = Fe, Co, Ni), *J. Phys. Chem. C* 115 (2011) 4971–4979.
- [23] M.G. Hu, R.A. Geanangel, W.W. Wendlandt, The thermal decomposition of ammonia borane, *Thermochim. Acta* 23 (1978) 249–255.
- [24] C.R. Miranda, G. Ceder, *Ab initio* investigation of ammonia-borane complexes for hydrogen storage, *J. Chem. Phys.* 126 (2007) 184703, 1–10.
- [25] W.J. Shaw, J.C. Linehan, N.K. Szymczak, D.J. Heldebrant, C. Yonker, D.M. Camaioni, R.T. Baker, T. Autrey, *In situ* multinuclear NMR spectroscopic studies of the thermal decomposition of ammonia borane in solution, *Angew. Chem. Int. Ed.* 47 (2008) 7493–7496.
- [26] D.P. Kim, J. Economy, Occurrence of liquid crystallinity in a borazine polymer, *Chem. Mater.* 6 (1994) 395–400.
- [27] Y. Filinchuk, R. Cerny, H. Hagemann, Insight into Mg(BH<sub>4</sub>)<sub>2</sub> with synchrotron X-ray diffraction: structure revision, crystal chemistry, and anomalous thermal expansion, *Chem. Mater.* 21 (2009) 925–933.
- [28] C. Wu, G. Wu, Z. Xiong, W.I.F. David, K.R. Ryan, M.O. Jones, P.P. Edwards, H. Chu, P. Chen, Stepwise phase transition in the formation of lithium amidoborane, *Inorg. Chem.* 49 (2010) 4319–4323.
- [29] R.C. Garvie, The occurrence of metastable tetragonal zirconia as a crystallite size effect, *J. Phys. Chem.* 69 (1965) 1238–1243.
- [30] W. Stichert, F. Schüth, Influence of crystallite size on the properties of zirconia, *Chem. Mater.* 10 (1998) 2020–2026.